Letter

# Skyrmion and vortex crystals in the Hubbard model

Kaito Kobayashi [1] and Satoru Hayami [2]
[1]*Department of Applied Physics, The University of Tokyo, Tokyo 113-8656, Japan*
[2]*Graduate School of Science, Hokkaido University, Sapporo 060-0810, Japan*

(Received 3 August 2022; accepted 5 October 2022; published 20 October 2022)

A mutual interplay between the charge and spin degrees of freedom in itinerant magnets leads to a plethora of topological spin textures, such as magnetic skyrmion and vortex crystals, in both centrosymmetric and noncentrosymmetric hosts. Meanwhile, their stabilization has been extensively studied in a system including classical localized spins. We here study a realization of the skyrmion crystal in a centrosymmetric triangular-lattice Hubbard model, where the itinerant nature of electrons plays a more significant role. By performing self-consistent mean-field calculations, we find that two types of skyrmion crystals with spatially nonuniform charge modulations appear in the ground state at zero magnetic field. Moreover, we obtain another noncoplanar vortex crystal phase without a net scalar chirality in the vicinity of the skyrmion crystal phase. We show that the latter vortex crystal exhibits a topological phase transition to a different skyrmion phase in an applied magnetic field. Our results provide a possibility of skyrmion and vortex crystals in itinerant magnets without localized moments.

DOI: 10.1103/PhysRevB.106.L140406

Itinerant magnets manifest themselves not only in various magnetic orderings but also in unusual conductive phenomena as a consequence of the synergy between charge and spin degrees of freedom in electrons. The microscopic mechanisms of magnetically ordered phases are often different from those in insulating magnets; an effective interaction through the kinetic motion of electrons as well as the Coulomb interaction plays an important role in determining optimal spin configurations. A typical example is the Ruderman-Kittel-Kasuya-Yosida (RKKY) interaction [1–3], which leads to the instability toward helical magnetic ordering with a long period structure featured by a single-$Q$ modulation. Furthermore, such a spin-charge entanglement brings about a comparable higher-order multiple-spin interaction to the RKKY interaction depending on the electronic band structures, which results in noncoplanar magnetic orderings characterized by a superposition of single-$Q$ helical states, i.e., a multiple-$Q$ state [4–13]. These nontrivial spin textures are the source of nontrivial conductive phenomena even without relativistic spin-orbit coupling, such as the topological Hall effect [14–20] and nonreciprocal transport [21–24].

Recently, it was revealed that a magnetic skyrmion crystal (SkX), which has a topologically protected noncoplanar spin texture, is also realized by the itinerant nature of electrons based on the analysis for the Kondo lattice model consisting of itinerant electrons and classical localized spins [25,26]. Subsequently, the emergence of the SkX is accounted for by an effective spin model with a positive biquadratic interaction in addition to the RKKY interaction, which originates from the Fermi-surface instability [27]. As this mechanism can be applied to any lattice structures irrespective of spatial inversion symmetry, it might provide the microscopic origin of the SkXs observed in centrosymmetric magnets, such as $Gd_2PdSi_3$ [28–32]. Indeed, magnetic phase diagrams in centrosymmetric skyrmion-hosting materials have been reproduced by the effective spin model, such as $GdRu_2Si_2$ [33–35], $Gd_3Ru_4Al_{12}$ [36,37], and $EuAl_4$ [38–41].

Meanwhile, there is a natural question about whether or not the SkX remains robust when electrons show an itinerant nature rather than a localized one. In other words, it is unclear whether the instability toward the SkX occurs by the kinetic motion of electrons even without a classical spin degree of freedom. To answer this question, we investigate the Hubbard model without localized spins. Based on self-consistent mean-field calculations for the Hubbard model on a centrosymmetric triangular lattice, we show that two types of the SkX appear even without an external magnetic field, as found in the Kondo lattice model [25], although the spin amplitudes are much smaller and strongly depend on the site. In addition, we discover a triple-$Q$ ($3Q$) vortex phase without a spin scalar chirality that was not reported as the ground state in the Kondo lattice model. We show that the magnetic field causes a topological phase transition from the $3Q$ vortex phase to another SkX phase. Our results indicate the importance of the charge degree of freedom, which will become a source of not only the SkX but also different types of vortex phases in itinerant magnets.

Let us consider the Hubbard model on a two-dimensional triangular lattice, which is given by

$$\mathcal{H} = -\sum_{ij\sigma} t_{ij} c^{\dagger}_{i\sigma} c_{j\sigma} + U \sum_{i} n_{i\uparrow} n_{i\downarrow} - B \sum_{i} S^{z}_{i}, \qquad (1)$$

where the operator $c^{\dagger}_{i\sigma}$ ($c_{i\sigma}$) is a creation (annihilation) operator for an electron with spin $\sigma$ at site $i$. The first term describes the kinetic energy of the electrons with the transfer

 

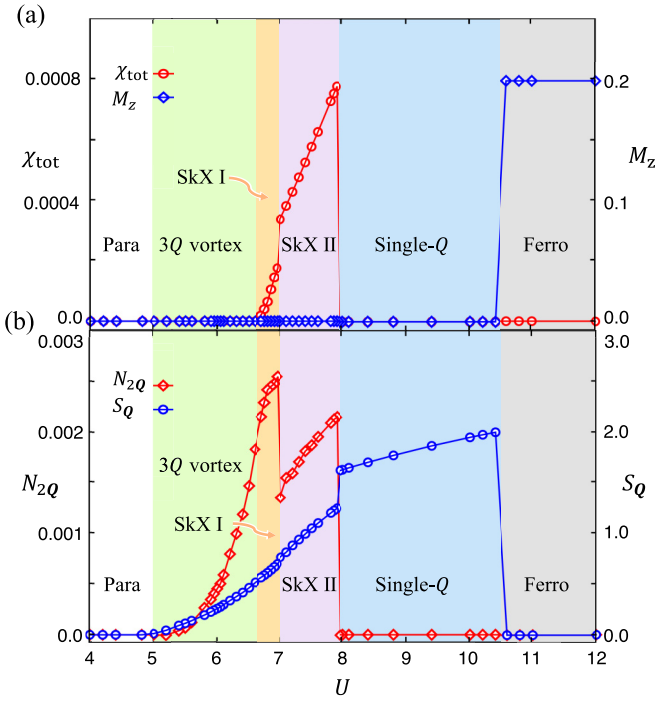


FIG. 1. $U$ dependence of (a) the total scalar chirality $\chi_{\rm tot}$ and the magnetization $M_z$, and (b) the charge structure factor $N_{2\boldsymbol{Q}}$ and the spin structure factor $S_{\boldsymbol{Q}}$ summed over $2\boldsymbol{Q}_\mu$ and $\boldsymbol{Q}_\mu$, respectively. The different colors in the background represent the different phases.

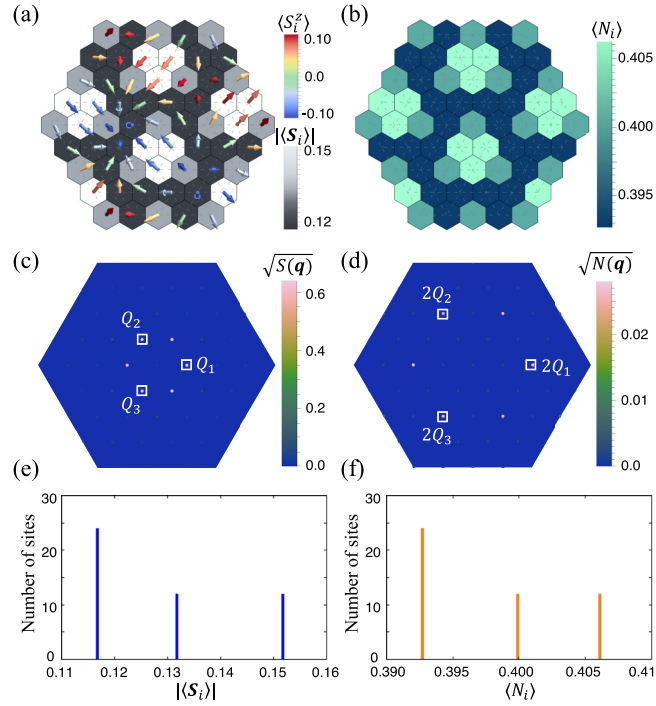


FIG. 2. (a) Real-space spin configuration in the SkX II phase at $U = 7.8$. The arrows represent the spins, their colors display the $z$-spin component, and the contour shows the spin norm $|\langle \boldsymbol{S}_i\rangle|$. (b) The contour plot for the charge density. (c), (d) The intensity plot of the square root of (c) the spin structure factor $S(\boldsymbol{q})$ and (d) the charge structure factor $N(\boldsymbol{q})$. (e) The histogram of $|\langle \boldsymbol{S}_i\rangle|$ with a bin width of 0.0005. (f) The histogram of $\langle N_i\rangle$ with a bin width of 0.0002.

integral between sites $i$ and $j$, $t_{ij}$, that typically take around $10^0$–$10^2$ meV depending on the itinerancy of the electrons. The second term represents the on-site Coulomb interaction with the coupling constant $U$ where $n_{i\sigma} = c^\dagger_{i\sigma}c_{i\sigma}$. The third term represents the Zeeman coupling to an external field along the $z$ direction: $S^z_i = \frac{1}{2}(c^\dagger_{i\uparrow}c_{i\uparrow} - c^\dagger_{i\downarrow}c_{i\downarrow})$.

In the following calculations, we consider the nearest-neighbor hopping, $t_1 = 1$ (energy unit of the model), and third-neighbor hopping, $t_3 = -0.85$, since these hopping parameters lead to a Fermi-surface instability at the commensurate wave vectors, $\boldsymbol{Q}_1 = (\pi/3, 0)$, $\boldsymbol{Q}_2 = (-\pi/6, \sqrt{3}\pi/6)$, and $\boldsymbol{Q}_3 = (-\pi/6, -\sqrt{3}\pi/6)$ for the electron filling $n_i \equiv \sum_\sigma n_{i\sigma} \simeq 0.398$ [27] (the lattice constant of the triangular lattice is set as unity); the instability toward the SkX with $3Q$ modulation at $\boldsymbol{Q}_1$–$\boldsymbol{Q}_3$ has been found in the Kondo lattice model with classical localized spins [25].

For the model in Eq. (1), we perform self-consistent mean-field calculations at zero temperature based on the Hartree-Fock approximation for the Coulomb interaction: $\sum_i n_{i\uparrow}n_{i\downarrow} \simeq \langle n_{i\downarrow}\rangle n_{i\uparrow} + \langle n_{i\uparrow}\rangle n_{i\downarrow} - \langle n_{i\uparrow}\rangle\langle n_{i\downarrow}\rangle - \langle c^\dagger_{i\downarrow}c_{i\uparrow}\rangle c^\dagger_{i\uparrow}c_{i\downarrow} - \langle c^\dagger_{i\uparrow}c_{i\downarrow}\rangle c^\dagger_{i\downarrow}c_{i\uparrow} + \langle c^\dagger_{i\uparrow}c_{i\downarrow}\rangle\langle c^\dagger_{i\downarrow}c_{i\uparrow}\rangle$.

We consider the magnetically ordered states in an $N_{\rm m} = 48$-site magnetic unit cell under periodic boundary conditions to accommodate the SkX with $\boldsymbol{Q}_1$–$\boldsymbol{Q}_3$ [see also Fig. 2(a) for the definition of the magnetic unit cell]. In order to reduce the finite-size effect, we introduce supercells made of $N_{\boldsymbol{k}} = 60 \times 60$ magnetic unit cells. Almost the same results are obtained for $N_{\boldsymbol{k}} = 32 \times 32$, which indicates the size dependence is almost negligible. The convergent condition is determined by $\Delta(\langle c^\dagger_{i\sigma}c_{i\sigma'}\rangle) < 10^{-8}$ for each site $i$ and spin $\sigma$.

Once the convergent spin configurations are obtained, we examine the spin and charge properties by calculating the spin and charge structure factors, $S(\boldsymbol{q})$ and $N(\boldsymbol{q})$, respectively, which are given by

$$S(\boldsymbol{q}) = \frac{1}{N}\sum_{ij}\langle \boldsymbol{S}_i\rangle \cdot \langle \boldsymbol{S}_j\rangle e^{i\boldsymbol{q}\cdot(\boldsymbol{r}_i - \boldsymbol{r}_j)}, \tag{2}$$

$$N(\boldsymbol{q}) = \frac{1}{N}\sum_{ij}\Delta n_i \Delta n_j e^{i\boldsymbol{q}\cdot(\boldsymbol{r}_i - \boldsymbol{r}_j)}, \tag{3}$$

where $\boldsymbol{r}_i$ is the position vector at site $i$ in the larger magnetic unit cell for $N = 12 \times 12 = 3N_{\rm m}$ sites corresponding to a modulation period of $\pi/6$; $\Delta n_i \equiv \sum_\alpha \langle c^\dagger_{i\alpha}c_{i\alpha}\rangle - n_{\rm ave}$ with the average charge density $n_{\rm ave}$. We also calculate the total magnetization per site $M_z = \sum_i \langle S^z_i\rangle/N_{\rm m}$. In addition, to identify whether or not the obtained states are topologically trivial, we compute the scalar spin chirality per triangle in the magnetic unit cell, $\chi_{\rm tot} = \sum_{\{ijk\}}\langle \boldsymbol{S}_i\rangle \cdot (\langle \boldsymbol{S}_j\rangle \times \langle \boldsymbol{S}_k\rangle)/2N_{\rm m}$. The nonzero value of $\chi_{\rm tot}$ becomes the origin of the topological Hall effect [14].

Figure 1 shows the ground-state phase diagram against $U$ at a zero field, i.e., $B = 0$. There are six phases characterized by different spin, charge, and chirality quantities. We show the $U$ dependence of $\chi_{\rm tot}$ and $M_z$ in Fig. 1(a) and the sum of the structure factors at the commensurate wave vectors $\boldsymbol{Q}_\mu$ and $2\boldsymbol{Q}_\mu$, $N_{2\boldsymbol{Q}} \equiv \sum_\mu N(2\boldsymbol{Q}_\mu)$ and $S_{\boldsymbol{Q}} \equiv \sum_\mu S(\boldsymbol{Q}_\mu)$, in Fig. 1(b). In the weak(strong)-correlation regime, the paramagnetic (ferromagnetic) state is realized, whose tendency

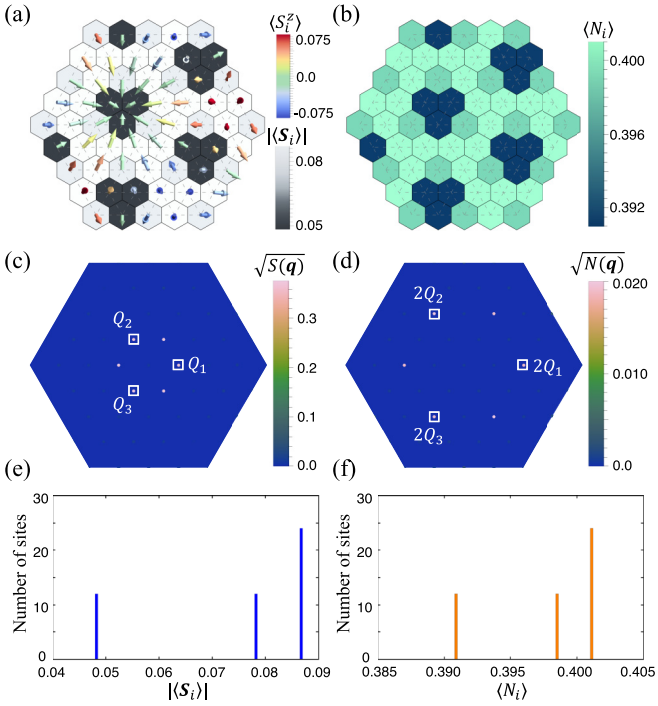


FIG. 3. The same plots as in Fig. 2 in the $3Q$ vortex phase at $U = 6.4$.

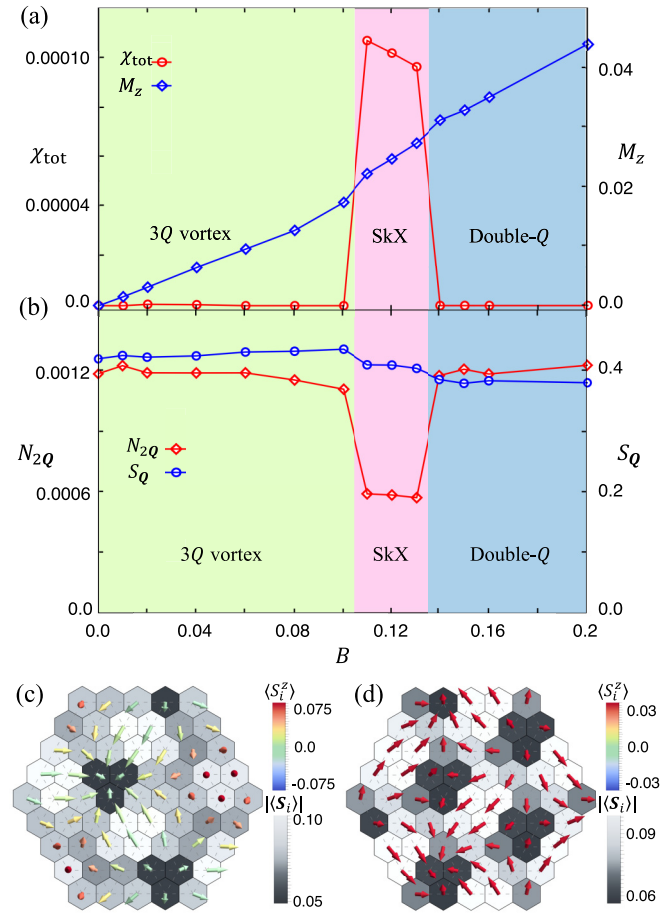


FIG. 4. $B$ dependence of (a) $\chi_{\rm tot}$ and $M_z$, and (b) $N_{2\boldsymbol{Q}}$ and $S_{\boldsymbol{Q}}$. (c), (d) The spin configurations in (c) the SkX phase at $B = 0.12$ and (d) the double-$Q$ phase at $B = 0.16$.

has been found in the Hubbard model [42,43]. Meanwhile, in the intermediate-correlation regime, we obtain four magnetic phases. Among them, three out of the four are characterized by multiple-$Q$ states: the $3Q$ vortex phase, SkX I, and SkX II. The remaining single-$Q$ state next to the ferromagnetic state is characterized by the single-$Q$ spiral state with $S_{\boldsymbol{Q}}$ but without $\chi_{\rm tot}$, $M_z$, and $N_{2\boldsymbol{Q}}$.

For $7.0 \lesssim U \lesssim 7.9$, we find that the SkX II with nonzero $\chi_{\rm tot}$ but zero $M_z$ becomes the ground state, as shown in Fig. 1(a). This state has triple-$Q$ charge and spin modulations, as shown in Fig. 1(b). Indeed, almost the same intensities at $\boldsymbol{Q}_\mu$ ($2\boldsymbol{Q}_\mu$) are observed in the spin (charge) structure factor, as shown in Figs. 2(c) and 2(d). It is noted that the triple-$Q$ peak structure in $N(\boldsymbol{q})$ is driven by the triple-$Q$ spin density waves. The peak position at $2\boldsymbol{Q}_\mu$ indicates that the constituent spin density waves propagate in an orthogonal way in spin space [44,45]. The equal triple-$Q$ intensities in $S(\boldsymbol{q})$ and $N(\boldsymbol{q})$ appear in the real-space spin and charge distributions in Figs. 2(a) and 2(b), respectively; both $|\langle \boldsymbol{S}_i \rangle|$ and $\langle N_i \rangle$ are distributed in a threefold-symmetric way. In addition, we find that both of them exhibit three discrete values, as shown in Figs. 2(e) and 2(f), which means that there are three independent environments in the SkX II phase. This phase presumably corresponds to the SkX stabilized in the Kondo lattice model [25].

On the other hand, for $5.0 \lesssim U \lesssim 6.6$, the $3Q$ vortex phase is stabilized, which also exhibits triple-$Q$ charge and spin modulations [Figs. 1(b), 3(c), and 3(d)] but no $\chi_{\rm tot}$ and $M_z$ [Fig. 1(a)]; the charge modulation at $2\boldsymbol{Q}_\mu$ indicates a similar multiple-$Q$ superposition to the SkX II. In addition, the absence of $\chi_{\rm tot}$ suggests the occurrence of the phase shift among the constituent waves from the SkX II [46–48], which has been found at finite temperatures in the Kondo lattice model [46]. The real-space spin configuration is characterized by four different spin vortices where the spin norm $|\langle \boldsymbol{S}_i \rangle|$ becomes small, as shown in Fig. 3(a). Accordingly, the charge distribution is also threefold symmetric around the vortices with small $|\langle N_i \rangle|$, as shown in Fig. 3(b). The histograms of $|\langle \boldsymbol{S}_i \rangle|$ [Fig. 3(e)] and $\langle N_i \rangle$ [Fig. 3(f)] show the opposite tendency to the SkX II in Figs. 2(e) and 2(f); the sites with larger $|\langle \boldsymbol{S}_i \rangle|$ and $\langle N_i \rangle$ are preferred in the $3Q$ vortex. The ratio of maximum and minimum values of $|\langle \boldsymbol{S}_i \rangle|$ is around 0.56, which is much smaller than that of the SkX II phase 0.77, while the ratio in terms of $\langle N_i \rangle$ takes similar values: 0.975 for the $3Q$ vortex and 0.967 for the SkX II. This result implies that the site-dependent moment reduction due to the kinetic motion of electrons, i.e., the charge degree of freedom, is important for the realization of the $3Q$ vortex as the ground state [49].

In the narrow region sandwiched by the $3Q$ vortex and the SkX II, the SkX I appears. Although this state shows a nonzero scalar chirality as the SkX II, its spin and charge structure factors appear to be continuously connected from the $3Q$ vortex phase, as shown in Figs. 1(a) and 1(b). In addition, the spin norm and charge density take four discrete values, which suggests the SkX I phase has a lower symmetry than the $3Q$ vortex and SkX II phases with three independent

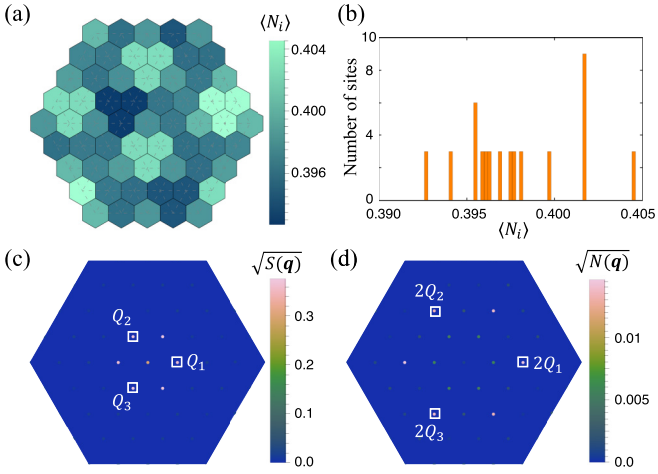


FIG. 5. The data of the SkX phase at $B = 0.12$. (a) The charge density distribution in real space. (b) The histogram of $\langle N_i \rangle$ with a bin width of 0.0002. (c), (d) The intensity plot of the square root of (c) $S(\boldsymbol{q})$ and (d) $N(\boldsymbol{q})$.

environments. Thus, the SkX I is regarded as the intermediate state between the $3Q$ vortex and SkX II.

Let us compare the present results with those in the Kondo lattice model [25]. In both models, the SkXs characterized by the triple-$Q$ structures in $S(\boldsymbol{q})$ and $N(\boldsymbol{q})$ are stabilized at zero field, but a distinct difference between them is found in the spin norm. The SkX II in the Hubbard model shows a strong spatial dependence of $|\langle \boldsymbol{S}_i \rangle|$ [Fig. 2(a)] in contrast to the case of the Kondo lattice model with fixed-length classical spins. This indicates that the itinerant character appears more clearly in the Hubbard model. Such a qualitative difference might be the origin of another triple-$Q$ vortex phase in Fig. 3(a), which is not stabilized as the ground state in the Kondo lattice model due to the constraint in terms of the spin norm. Thus, the interplay between the charge and spin degrees of freedom plays an important role in inducing noncoplanar multiple-$Q$ states, which will bring about further exotic spin-charge entangled topological spin textures.

Next, we consider the effect of the magnetic field $B$ on the $3Q$ vortex phase. Figure 4(a) shows the $B$ dependence of $\chi_{\rm tot}$ and $M_z$, while Fig. 4(b) shows that of $N_{2\boldsymbol{Q}}$ and $S_{\boldsymbol{Q}}$ at $U = 6.4$. When introducing $B$, $M_z$ becomes nonzero and linearly increases in the $3Q$ vortex phase in Fig. 4(a). While increasing $B$, $\chi_{\rm tot}$ jumps to nonzero values at $B = 0.11$, which implies the appearance of the SkX phase. The obtained SkX spin configuration is shown in Fig. 4(c). Compared with the SkX II in Fig. 2(a), the spatial distributions of $|\langle \boldsymbol{S}_i \rangle|$ in Fig. 4(c) and $\langle N_i \rangle$ in Fig. 5(a) are more complicated; indeed, the histogram of $\langle N_i \rangle$ exhibits multiple values, as shown in Fig. 5(b). Accordingly, additional intensities appear at $\boldsymbol{Q}_\mu$ and $\boldsymbol{Q}_\mu - \boldsymbol{Q}_{\mu'}$ in $N(\boldsymbol{q})$ in Fig. 5(d). Owing to the multiple peak structures in $N(\boldsymbol{q})$, the intensity of $N_{2\boldsymbol{Q}}$ becomes small compared to that of the $3Q$ vortex, as shown in Fig. 4(b). In addition, this state exhibits a nonzero net magnetization owing to the magnetic field; see also the $\boldsymbol{q} = \boldsymbol{0}$ component in the spin structure factor in Fig. 5(c). Thus, this SkX phase induced by the magnetic field is qualitatively different from the SkX I and SkX II obtained at zero field, where only the former SkX exhibits nonzero net magnetization and nonzero $N(\boldsymbol{Q}_\mu)$. Since a further increase of $B$ suppresses the $z$-spin modulation in the SkX, the spin state turns into the double-$Q$ state with the in-plane double-$Q$ modulated spin structure shown in Fig. 4(d). In the double-$Q$ state, $N(\boldsymbol{q})$ shows peaks at two out of three $2\boldsymbol{Q}_\mu$ as does the $3Q$ vortex, whose amplitude is comparable to each other [Fig. 4(b)].

Meanwhile, there is no instability toward such a field-induced SkX in the case of SkX II. In this case, the SkX II phase turns into another vortex phase with a skyrmion number of 0 at $B = 0.065$, whose spin and charge modulations are similar to those found in the Kondo lattice model at high fields [25].

It is noteworthy to mention that the obtained SkX under the magnetic field in Fig. 5 is qualitatively different from the SkX found in the Kondo lattice model [25] and other spin models. By closely looking into the spin configuration of the SkX phase in Fig. 4(c), one finds that almost all the spins have a positive $\langle S_i^z \rangle$ and only a few spins around the two skyrmion cores where $|\langle \boldsymbol{S}_i \rangle|$ becomes small have a slight negative $\langle S_i^z \rangle$. These two skyrmion cores yield a winding number of $+1$, i.e., a skyrmion number of $-0.5$, which reflects the slight negative $\langle S_i^z \rangle$ at the core. Intriguingly, in this phase, there is another vortex core, where the spin is almost parallel to the $+z$ direction in the middle right-hand side of the spin configuration. This vortex accompanies the winding number of $-2$, i.e., the skyrmion number of $-1$. In the end, the total skyrmion number in the magnetic unit cell is given by $-2$. This is in contrast to the SkX in the Kondo lattice model, where the $z$-spin component of the skyrmion core points along $S_i^z = -1$ and the spin configuration possesses a skyrmion number of $-1$ [25]. Reflecting such a difference, an intriguing excitation spectrum, such as the separation of spin and charge excitations [45,50], might be expected in the present SkX phases, which is left for future study.

To summarize, we have studied the ground-state spin configurations in the Hubbard model on a centrosymmetric triangular lattice with an emphasis on the itinerant nature of electrons. Based on the mean-field analysis, we have discovered several multiple-$Q$ phases including the SkX and vortex phases in the presence of strong spin-charge entanglement. Our discovery indicates that itinerant magnets provide a variety of topological spin crystals even without the classical localized spins, and suggests the experimental feasibility of multiple-$Q$ states in centrosymmetric materials consisting of $d$ and $5f$ electrons with an itinerant character. This result provides a further possibility to search for exotic topological magnetism.

We thank R. Yambe and M. Yatsushiro for fruitful discussions. This research was supported by JSPS KAKENHI Grants No. JP21H01037, No. JP22H04468, No. JP22H00101, No. JP22H01183, and by JST PRESTO (JPMJPR20L8). K.K. was supported by the Program for Leading Graduate Schools (MERIT-WINGS).

[1] M. A. Ruderman and C. Kittel, Indirect exchange coupling of nuclear magnetic moments by conduction electrons, Phys. Rev. **96**, 99 (1954).

[2] T. Kasuya, A theory of metallic ferro- and antiferromagnetism on Zener's model, Prog. Theor. Phys. **16**, 45 (1956).

[3] K. Yosida, Magnetic properties of Cu-Mn alloys, Phys. Rev. **106**, 893 (1957).

[4] I. Martin and C. D. Batista, Itinerant Electron-Driven Chiral Magnetic Ordering and Spontaneous Quantum Hall Effect in Triangular Lattice Models, Phys. Rev. Lett. **101**, 156402 (2008).

[5] Y. Akagi and Y. Motome, Spin chirality ordering and anomalous Hall effect in the ferromagnetic Kondo lattice model on a triangular lattice, J. Phys. Soc. Jpn. **79**, 083711 (2010).

[6] G.-W. Chern, Noncoplanar Magnetic Ordering Driven by Itinerant Electrons on the Pyrochlore Lattice, Phys. Rev. Lett. **105**, 226403 (2010).

[7] Y. Akagi, M. Udagawa, and Y. Motome, Hidden Multiple-Spin Interactions as an Origin of Spin Scalar Chiral Order in Frustrated Kondo Lattice Models, Phys. Rev. Lett. **108**, 096401 (2012).

[8] D. Solenov, D. Mozyrsky, and I. Martin, Chirality Waves in Two-Dimensional Magnets, Phys. Rev. Lett. **108**, 096403 (2012).

[9] S. Hayami and Y. Motome, Multiple-$Q$ instability by $(d-2)$-dimensional connections of Fermi surfaces, Phys. Rev. B **90**, 060402(R) (2014).

[10] K. Barros, J. W. F. Venderbos, G.-W. Chern, and C. D. Batista, Exotic magnetic orderings in the kagome Kondo-lattice model, Phys. Rev. B **90**, 245119 (2014).

[11] R. Ozawa, S. Hayami, K. Barros, G.-W. Chern, Y. Motome, and C. D. Batista, Vortex crystals with chiral stripes in itinerant magnets, J. Phys. Soc. Jpn. **85**, 103703 (2016).

[12] C. D. Batista, S.-Z. Lin, S. Hayami, and Y. Kamiya, Frustration and chiral orderings in correlated electron systems, Rep. Prog. Phys. **79**, 084504 (2016).

[13] Z. Wang and C. D. Batista, Skyrmion crystals in the triangular Kondo lattice model, arXiv:2111.13976.

[14] K. Ohgushi, S. Murakami, and N. Nagaosa, Spin anisotropy and quantum Hall effect in the kagomé lattice: Chiral spin state based on a ferromagnet, Phys. Rev. B **62**, R6065 (2000).

[15] R. Shindou and N. Nagaosa, Orbital Ferromagnetism and Anomalous Hall Effect in Antiferromagnets on the Distorted fcc Lattice, Phys. Rev. Lett. **87**, 116801 (2001).

[16] N. A. Sinitsyn, Semiclassical theories of the anomalous Hall effect, J. Phys.: Condens. Matter **20**, 023201 (2008).

[17] A. Neubauer, C. Pfleiderer, B. Binz, A. Rosch, R. Ritz, P. G. Niklowitz, and P. Böni, Topological Hall Effect in the $A$ Phase of MnSi, Phys. Rev. Lett. **102**, 186602 (2009).

[18] M. Lee, W. Kang, Y. Onose, Y. Tokura, and N. P. Ong, Unusual Hall Effect Anomaly in MnSi under Pressure, Phys. Rev. Lett. **102**, 186601 (2009).

[19] N. Nagaosa, J. Sinova, S. Onoda, A. H. MacDonald, and N. P. Ong, Anomalous hall effect, Rev. Mod. Phys. **82**, 1539 (2010).

[20] D. Xiao, M.-C. Chang, and Q. Niu, Berry phase effects on electronic properties, Rev. Mod. Phys. **82**, 1959 (2010).

[21] Y. Tokura and N. Nagaosa, Nonreciprocal responses from non-centrosymmetric quantum materials, Nat. Commun. **9**, 3740 (2018).

[22] S. Hayami, Y. Yanagi, and H. Kusunose, Bottom-up design of spin-split and reshaped electronic band structures in antiferromagnets without spin-orbit coupling: Procedure on the basis of augmented multipoles, Phys. Rev. B **102**, 144441 (2020).

[23] S. Hayami and M. Yatsushiro, Nonlinear nonreciprocal transport in antiferromagnets free from spin-orbit coupling, Phys. Rev. B **106**, 014420 (2022).

[24] S. Hayami and M. Yatsushiro, Nonreciprocal transport in noncoplanar magnetic systems without spin-orbit coupling, net scalar chirality, or magnetization, J. Phys. Soc. Jpn. **91**, 094704 (2022).

[25] R. Ozawa, S. Hayami, and Y. Motome, Zero-Field Skyrmions with a High Topological Number in Itinerant Magnets, Phys. Rev. Lett. **118**, 147205 (2017).

[26] S. Hayami and Y. Motome, Topological spin crystals by itinerant frustration, J. Phys.: Condens. Matter **33**, 443001 (2021).

[27] S. Hayami, R. Ozawa, and Y. Motome, Effective bilinear-biquadratic model for noncoplanar ordering in itinerant magnets, Phys. Rev. B **95**, 224424 (2017).

[28] T. Kurumaji, T. Nakajima, M. Hirschberger, A. Kikkawa, Y. Yamasaki, H. Sagayama, H. Nakao, Y. Taguchi, T.-h. Arima, and Y. Tokura, Skyrmion lattice with a giant topological Hall effect in a frustrated triangular-lattice magnet, Science **365**, 914 (2019).

[29] E. V. Sampathkumaran, A report of (topological) Hall anomaly two decades ago in $Gd_2PdSi_3$, and its relevance to the history of the field of topological Hall effect due to magnetic skyrmions, arXiv:1910.09194.

[30] T. Nomoto, T. Koretsune, and R. Arita, Formation Mechanism of the Helical $\boldsymbol{Q}$ Structure in Gd-Based Skyrmion Materials, Phys. Rev. Lett. **125**, 117204 (2020).

[31] J. A. M. Paddison, B. K. Rai, A. F. May, S. A. Calder, M. B. Stone, M. D. Frontzek, and A. D. Christianson, Magnetic Interactions of the Centrosymmetric Skyrmion Material $Gd_2PdSi_3$, Phys. Rev. Lett. **129**, 137202 (2022).

[32] J. Bouaziz, E. Mendive-Tapia, S. Blügel, and J. B. Staunton, Fermi-Surface Origin of Skyrmion Lattices in Centrosymmetric Rare-Earth Intermetallics, Phys. Rev. Lett. **128**, 157206 (2022).

[33] N. D. Khanh, T. Nakajima, X. Yu, S. Gao, K. Shibata, M. Hirschberger, Y. Yamasaki, H. Sagayama, H. Nakao, L. Peng, K. Nakajima, R. Takagi, T.-h. Arima, Y. Tokura, and S. Seki, Nanometric square skyrmion lattice in a centrosymmetric tetragonal magnet, Nat. Nanotechnol. **15**, 444 (2020).

[34] Y. Yasui, C. J. Butler, N. D. Khanh, S. Hayami, T. Nomoto, T. Hanaguri, Y. Motome, R. Arita, T.-h. Arima, Y. Tokura, and S. Seki, Imaging the coupling between itinerant electrons and localised moments in the centrosymmetric skyrmion magnet $GdRu_2Si_2$, Nat. Commun. **11**, 5925 (2020).

[35] N. D. Khanh, T. Nakajima, S. Hayami, S. Gao, Y. Yamasaki, H. Sagayama, H. Nakao, R. Takagi, Y. Motome, Y. Tokura, T.-h. Arima, and S. Seki, Zoology of multiple-Q spin textures in a centrosymmetric tetragonal magnet with itinerant electrons, Adv. Sci. **9**, 2105452 (2022).

[36] M. Hirschberger, T. Nakajima, S. Gao, L. Peng, A. Kikkawa, T. Kurumaji, M. Kriener, Y. Yamasaki, H. Sagayama, H. Nakao, K. Ohishi, K. Kakurai, Y. Taguchi, X. Yu, T.-h. Arima, and Y. Tokura, Skyrmion phase and competing magnetic orders on a breathing kagome lattice, Nat. Commun. **10**, 5831 (2019).

[37] M. Hirschberger, S. Hayami, and Y. Tokura, Nanometric skyrmion lattice from anisotropic exchange interactions in a centrosymmetric host, New J. Phys. **23**, 023039 (2021).

[38] T. Shang, Y. Xu, D. J. Gawryluk, J. Z. Ma, T. Shiroka, M. Shi, and E. Pomjakushina, Anomalous Hall resistivity and possible topological Hall effect in the $EuSl_4$ antiferromagnet, Phys. Rev. B **103**, L020405 (2021).

[39] R. Takagi, N. Matsuyama, V. Ukleev, L. Yu, J. S. White, S. Francoual, J. R. L. Mardegan, S. Hayami, H. Saito, K. Kaneko, K. Ohishi, Y. Ōnuki, T.-h. Arima, Y. Tokura, T. Nakajima, and S. Seki, Square and rhombic lattices of magnetic skyrmions in a centrosymmetric binary compound, Nat. Commun. **13**, 1472 (2022).

[40] S. Hayami, Multiple skyrmion crystal phases by itinerant frustration in centrosymmetric tetragonal magnets, J. Phys. Soc. Jpn. **91**, 023705 (2022).

[41] X. Y. Zhu, H. Zhang, D. J. Gawryluk, Z. X. Zhen, B. C. Yu, S. L. Ju, W. Xie, D. M. Jiang, W. J. Cheng, Y. Xu, M. Shi, E. Pomjakushina, Q. F. Zhan, T. Shiroka, and T. Shang, Spin order and fluctuations in the $EuAl_4$ and $EuGa_4$ topological antiferromagnets: A $\mu$SR study, Phys. Rev. B **105**, 014423 (2022).

[42] J. E. Hirsch, Two-dimensional Hubbard model: Numerical simulation study, Phys. Rev. B **31**, 4403 (1985).

[43] Y. Claveau, B. Arnaud, and S. D. Matteo, Mean-field solution of the Hubbard model: The magnetic phase diagram, Eur. J. Phys. **35**, 035023 (2014).

[44] S. Hayami and Y. Motome, Charge density waves in multiple-$Q$ spin states, Phys. Rev. B **104**, 144404 (2021).

[45] R. Eto, R. Pohle, and M. Mochizuki, Low-Energy Excitations of Skyrmion Crystals in a Centrosymmetric Kondo-Lattice Magnet: Decoupled Spin-Charge Excitations and Nonreciprocity, Phys. Rev. Lett. **129**, 017201 (2022).

[46] S. Hayami, T. Okubo, and Y. Motome, Phase shift in skyrmion crystals, Nat. Commun. **12**, 6927 (2021).

[47] S. Hayami and R. Yambe, Locking of skyrmion cores on a centrosymmetric discrete lattice: Onsite versus offsite, Phys. Rev. Res. **3**, 043158 (2021).

[48] K. Shimizu, S. Okumura, Y. Kato, and Y. Motome, Phase degree of freedom and topology in multiple-$Q$ spin textures, Phys. Rev. B **105**, 224405 (2022).

[49] Y. Kakehashi, D. Koja, T. Olonbayar, and H. Miyagi, Multiple helical spin density waves and magnetic skyrmions in itinerant electron system, J. Phys. Soc. Jpn. **87**, 094712 (2018).

[50] S. L. Sondhi, A. Karlhede, S. A. Kivelson, and E. H. Rezayi, Skyrmions and the crossover from the integer to fractional quantum Hall effect at small Zeeman energies, Phys. Rev. B **47**, 16419 (1993).